Experimental validation of a Bayesian model of visual acuity

Eugénie Dalimier Applied Optics Group, School of Physics, National University of Ireland, Galway, Ireland

Eliseo Pailos ICMA, Consejo Superior de Investigaciones Cientificas, Universidad de Zaragoza, Spain, & Departamento de Fisica Aplicada, Universidade de Santiago de Compostela, Spain

Ricardo Rivera ICMA, Consejo Superior de Investigaciones Cientificas, Universidad de Zaragoza, Spain

Rafael Navarro ICMA, Consejo Superior de Investigaciones Cientificas, Universidad de Zaragoza, Spain

Based on standard procedures used in optometry clinics, we compare measurements of visual acuity for 10 subjects (11 eyes tested) in the presence of natural ocular aberrations and different degrees of induced defocus, with the predictions given by a Bayesian model customized with aberrometric data of the eye. The absolute predictions of the model, without any adjustment, show good agreement with the experimental data, in terms of correlation and absolute error. The efficiency of the model is discussed in comparison with image quality metrics and other customized visual process models. An analysis of the importance and customization of each stage of the model is also given; it stresses the potential high predictive power from precise modeling of ocular and neural transfer functions.

Keywords: vision modeling, pattern recognition, ocular aberrations, best refraction, visual acuity

Citation: Dalimier, E., Pailos, E., Rivera, R., & Navarro, R. (2009). Experimental validation of a Bayesian model of visual acuity. *Journal of Vision, 9*(7):12, 1–16, http://journalofvision.org/9/7/12/, doi:10.1167/9.7.12.

Introduction

The introduction of rapid and precise aberrometry techniques in vision science (Liang, Grimm, Goelz, & Bille, 1994; Navarro & Losada, 1997) has recently sharpened and facilitated our knowledge of ocular optical aberrations. In the context of the development of refractive and cataract surgery techniques, particular attention has been given to these aberrations and their impact on visual performance, for example, to predict the changes incurred by the surgery. Based on individual aberrometric data, it is possible, through simple calculations, to model retinal image formation (Guirao, Porter, Williams, & Cox, 2002). One can also compute various metrics (Thibos, Hong, Bradley, & Applegate, 2004) to quantify the quality of the retinal image. Yet the prediction of the actual visual performance, typically given as the Snellen visual acuity in a clinical environment, implies the modeling of the entire visual processes including a pattern recognition task.

Recently, some of the authors presented the first partially customized model of Snellen visual acuity (Nestares, Navarro, & Antona, 2003). In this model, the ocular optical filtering is calculated from aberrometric data of the eye. The cortical response includes the retinal sampling and the filtering by a set of visual channels to which a neural contrast threshold curve is applied. A special feature of the model is the Bayesian approach of the pattern recognition stage. The assumption is made that the observer does not know the optical degradation of the possible templates, and the degradation is implicitly estimated by the Bayesian pattern recognition method. This operation is simplified by the visual channel decomposition. It introduces more robustness against the degradation due to optical aberrations than standard pattern recognition methods (Vargas, Campos, & Navarro, 2000). Preliminary results on one subject showed a close agreement between experimental measurements of visual acuity and the predictions given by the model (Nestares et al., 2003). Recently, more classical ideal observer models have also been customized to predict visual acuity or visual performance for other tests (Dalimier & Dainty, 2008; Watson & Ahumada, 2008), demonstrating the potential of customized visual process models.

doi: 10.1167/9.7.12 Received November 5, 2008; published July 21, 2009 ISSN 1534-7362

The present paper aims to provide a rigorous validation of our customized Bayesian model of visual acuity with a set of experimental data obtained for ten subjects (eleven eyes) with a large range of defocus amounts added to their natural ocular aberrations. These conditions reflect the standard procedures used in optometry clinics to measure visual performance and evaluate the best ophthalmic correction. In this work, it is also intended to provide a thorough analysis of the efficiency and limitations of the model and a new insight into the importance of each stage for vision modeling. The methods for the measurement of visual acuity, ocular aberrations, and model calculations will be detailed before the experimental results are compared to the predictions given by the model. The model will also be compared to different image quality metrics and other customized ideal observer models (Watson & Ahumada, 2008). Finally, we will investigate the importance of each feature and stage of the model to the overall output and further possibilities of improvement.

Methods

Subjects

Ten subjects participated in the study. The mean age was 30 years (standard deviation 7 years, range 22–48). The mean spherical equivalent (spherical + $\frac{1}{2}$ cylindrical refractive error) was −1.7 D (standard deviation 2.5 D, range −6.25 to 1.25 D). One subject, who had −5.25 D cylindrical error, was given a cylindrical correction during the tests; the other subjects were left uncorrected. The study followed the tenets of the Declaration of Helsinki and informed consent was obtained from the subjects after explanation of the nature and possible consequences of the study.

Ocular aberration measurements

The monochromatic ocular aberrations were measured with a custom-made laser ray tracing (LRT) system (Moreno-Barriuso & Navarro, 2000) for five of the subjects and with a commercial LRT system (Tracey Technologies) for the others. The principle of the LRT has been described elsewhere (Navarro & Losada, 1997) and will only be summarized here. A small laser collimated beam is sequentially scanned through the pupil, and the displaced spots formed on the retina are reimaged onto a camera to measure the local tilts introduced in the first pass of the light through the eye. The measurement wavelength for the custom-made LRT was 534 nm, while that for the commercial LRT is 632 nm. The measurements were performed for all subjects with their pupils dilated with Tropicamide 1%. The data could then be used to reconstruct the wavefront deformation over a given pupil diameter.

Visual acuity measurements

Visual acuity measurements were carried out for a number (between 8 and 15) of myopic states introduced with ophthalmic lenses, in steps of +0.25 D from the original prescription of the subject. A few points were also taken toward the hyperopic state to ensure that the best refractive state had been tested; however, the measurements were not extended in that direction to avoid compensation of refractive error by accommodation. For each refractive state, four measurements of visual acuity were performed.

The measurement procedure was the following. The subject was seated 6 m away from a liquid crystal display (LCD) where the black optotypes were shown on a bright white background (nominal luminance of 400 cd/m^2). The room was left bright to maintain natural pupil constriction. Visual acuity was measured with a simple staircase procedure and a letter identification task. The subject was asked to name optotypes among a reduced alphabet of 18 letters, which included the usual characters in commercial charts. The letters were generated using the Sloan font developed for the Pelli–Robson contrast sensitivity chart (Pelli, Robson, & Wilkins, 1988). The test started with a letter size easily recognizable by the subject. Four random optotypes were presented consecutively, and after at least three correct answers, the tested decimal visual acuity, VA = $1/10^{\text{logMAR}}$, was increased by 1/10. The process was repeated until the subject gave less than three correct answers, at which point the tested VA was decreased by half the step. The final VA value was given by the smallest letter size for which the subject passed the 75% threshold of correct responses. All the optotypes presented to the subject were recorded for later use in the model calculations.

The ophthalmic lenses used for the experiments introduced a magnification factor M_{RS} for the size of the retinal image. With the thin-lens approximation, M_{RS} can be calculated as

$$M_{RS} = \frac{1}{1 - sP_D}, \quad (1)$$

where s is the distance from the lens to the entrance pupil of the eye (it was measured to be 20 mm), and P_D is the power of the ophthalmic lens in diopters. To recover the retinal visual acuity of the subject, we divided the measured acuity by M_{RS}.

Finally, the optical aberrations (other than defocus) introduced by the ophthalmic lenses were fully characterized and found to be negligible.

Pupil diameter measurements

In order to implement the variations of the optical degradation in the model, the pupil size was constantly measured during the visual acuity tests with a custom-made digital pupillometer, as shown in Figure 1.

A camera was placed at a distance of 1 m from the pupil and an angle of 20° from the visual axis, not to obstruct the tested visual field of the subject. A ring of infrared (λ = 875 nm) LEDs mounted on the camera was used to illuminate the subject's pupil. The resolution of the system was ±0.14 mm for the measurement of the pupil diameter. The ophthalmic lenses placed in front of the pupil introduced a change in magnification of the pupil, which was taken into account by dividing the pupil diameter measurements by a factor M_P in fact equal to M_{RS} as defined in Equation 1. The mean pupil diameter measured for each letter size tested during the visual acuity measurements was stored for later use in the model computations. Hence, the fluctuation of the pupil diameter over the duration of the measurement and the effect on the optical degradation were taken into account in the model.

Numerical model calculations

The model calculation stages are well described in the paper by Nestares et al. (2003). They are shown again in Figure 2. One important aspect is that the numerical implementation of the model aims to mimic closely the experimental visual task performed by the subject during the visual acuity measurement. The same staircase procedure was used as in the experiments. The variations in the experimental conditions (optotypes presented and optical degradation affected by the changes of the pupil diameter) for each VA test were also simulated, as detailed below.

The numerical implementation was the following for each subject. For each letter size tested experimentally, the model observer was presented the same optotypes as those presented to the human observer. The spectrum of the object was filtered with the polychromatic optical

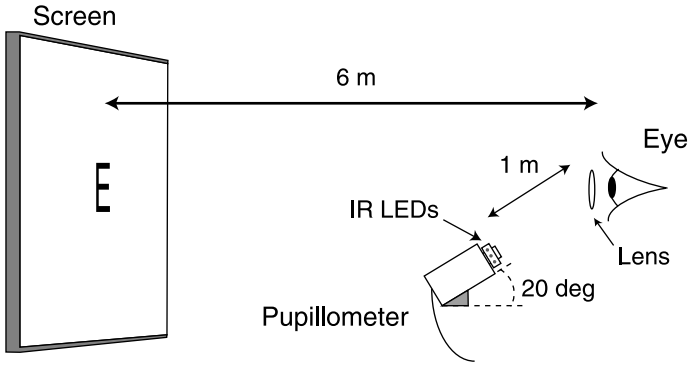

Figure 1. Setup for the simultaneous visual acuity tests and pupil diameter measurement.

transfer function (OTF_p) to compute the retinal image. First, the ocular aberrations of the dilated pupil were reconstructed over the mean pupil diameter measured when the particular letter size was tested. The monochromatic OTF, calculated from the wavefront map, was used to recover the OTF_p. The LCD used for the experiment had a broad color spectrum. Based on the literature (Llorente, Diaz-Santana, Lara-Saucedo, & Marcos, 2003), we assumed that the only ocular aberration significantly varying with wavelength in the visible is defocus, originating from the longitudinal chromatic aberration (LCA) of the human eye. As Yoon and Williams found similar effects of LCA on retinal image quality for both a broad spectrum display (a CRT in their case) and an equal energy spectrum (Yoon & Williams, 2002), we assumed a flat spectrum in our calculations. The monochromatic OTF was computed every 10 nm to cover the whole visible spectrum. The focused wavelength was taken to be 550 nm and we used the Indiana eye model (Thibos, Ye, Zhang, & Bradley, 1992) for the amount of LCA to be added at each wavelength. The effect of transverse chromatic aberration on the retinal image was ignored due to the high intersubject variability (Rynders, Lidkea, Chisholm, & Thibos, 1995) and the non-availability of data for our subjects. The sum of the monochromatic functions, weighted by the CIE standard observer photopic spectral sensitivity curve V_λ (Wyszecki & Stiles, 1982), gave the OTF_p.

The retinal sampling was modeled as a hexagonal structure with a frequency of 120 cycles/deg, based on anatomical estimates of cone density (Curcio, Sloan, Kalina, & Hendrickson, 1990). The sampled retinal image was then filtered by a set of channels to represent the cortical output (Nestares, Navarro, Portilla, & Tabernero, 1998). Gabor channels of one octave bandwidth, frequencies of 4, 8, 16, and 32 cycles/deg, and orientations of 0, 45, 90, and 135 deg were used. A contrast threshold, given by the inverse of a generic neural transfer function taken from previous measurements (Losada, Navarro, & Santamaría, 1993), was applied to the channel responses.

Finally, the pattern recognition stage was modeled with the assumption that the model observer does not know the optical degradation introduced by his eye. The cortical image $o_i(\mathbf{x})$ is compared against an approximation $a_i(\mathbf{x})$ of the degradation of the original optotype within each channel i, i.e.,

$$a_i(\mathbf{x}) = h_i c_i(\mathbf{x}-\mathbf{u}_i), \tag{2}$$

where $c(\mathbf{x})$ is the input object and $\{h_i, \mathbf{u}_i\}$ are the modulation and shift approximating the OTF_p within each channel, as given in Equation 7 in the original publication describing the model (Nestares et al., 2003). Practically, the observer finds the degradation parameters that maximizes the posterior probability $p(\{o_i\} \mid c, \{h_i, \mathbf{u}_i\})$ for each possible original optotype within each channel and selects the optotype giving the best maximum a posteriori

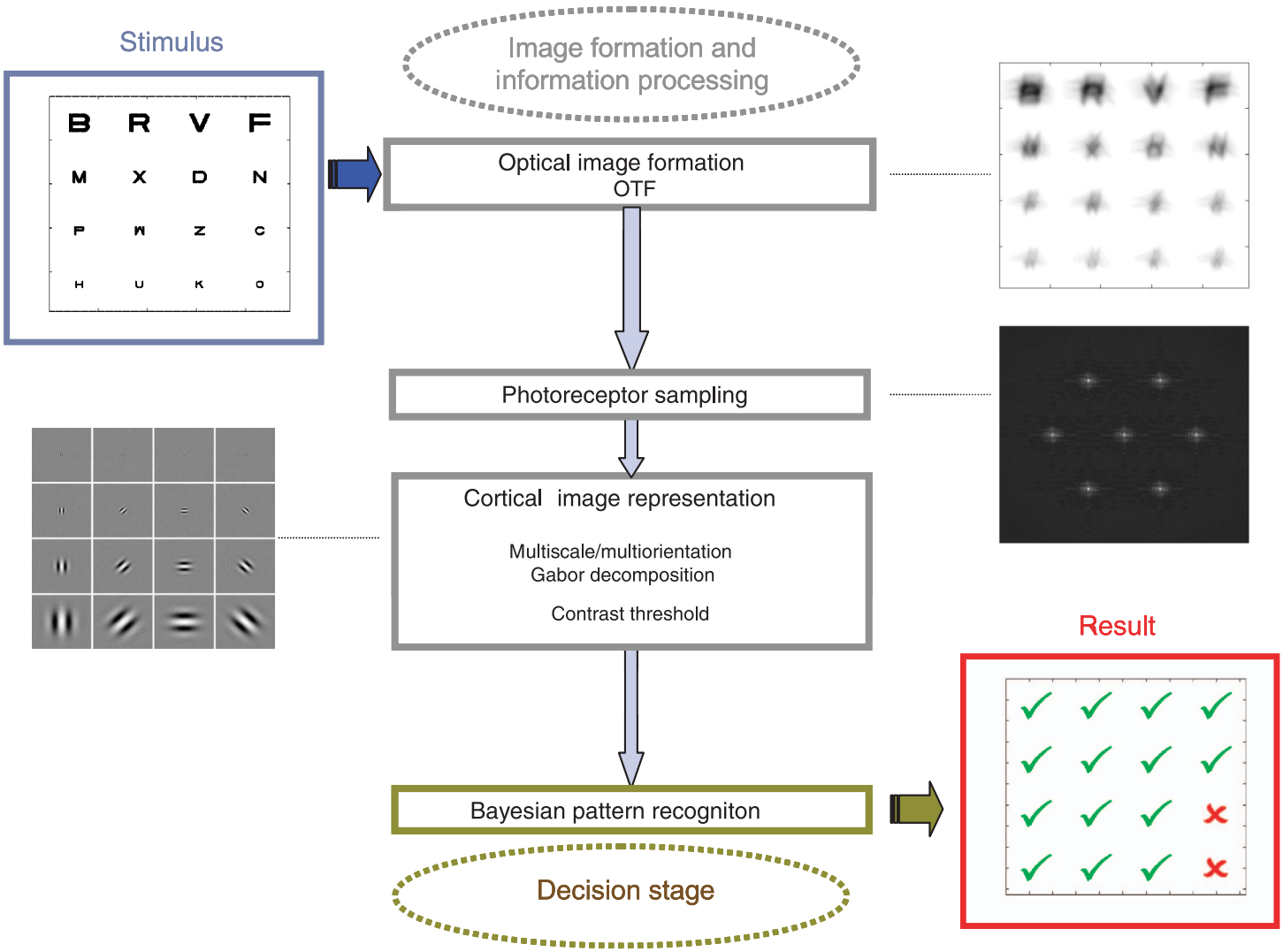

Figure 2. Schematic of the model calculations.

probability (MAP). Thus, the observer implicitly estimates the OTF_p sampled by the channels while estimating the optotype: This is a double Bayesian estimation. It was shown (Nestares et al., 2003) that maximizing the posterior probability for each input optotype j and channel is equivalent to calculating the value $\hat{\mathbf{u}}_i^j$ maximizing the correlation function

$$corr_i^j(\mathbf{u}_i) = \sum_{\mathbf{x}} o_i(\mathbf{x}) c_i^j(\mathbf{x}-\mathbf{u}_i), \tag{3}$$

and that the MAP for each optotype is given by

$$P_j \propto \sum_i \frac{\left[corr_i^j(\hat{\mathbf{u}}_i^j)\right]^2}{\sum_x \left[c_i^j(\mathbf{x})\right]^2}. \tag{4}$$

For each letter size, the responses of the model observer were compared to the correct responses, and the experimental threshold of correct responses (75%) was applied. Again, we used the staircase procedure to give a prediction of the visual acuity. The model calculations were performed four times as in the measurements, to take into account the variability due to the random selection of optotypes.

Evaluation of defocus

The characterization of the exact defocus term in the ocular wavefront maps is a difficult issue for several reasons. Firstly, the ocular wavefront measurements were performed at wavelengths of 534 nm and 632 nm for the custom-made and the commercial aberrometers, respectively, while the visual acuity tests were carried out with a wide visible spectrum. The known chromatic aberration of the human eye predicts a shift in defocus with the wavelength (Thibos et al., 1992). Furthermore, accommodation was left unparalyzed during the visual tests. The

subject could therefore adjust to the target vergence given by its final distance from the subject (6 m equivalent to 0.17 D). Finally, a certain additional amount of defocus might be present to balance the effects of his higher order aberrations and optimize the retinal image quality (Navarro, 2009; Yoon & Williams, 2002).

To address these issues, we adopted the following methodology. We first assumed a defocus term equal to 0 at the peak of experimental VA. For each refractive state, we performed the model calculations with a Zernike defocus coefficient equal to

$$cz_4 = \frac{r^2}{4\sqrt{3}}(D_{lens} - D_0), \quad (5)$$

where r is the pupil radius given in millimeters, D_{lens} is the power in diopters of the ophthalmic lens for each tested refractive state, D_0 is the power in diopters of the lens corresponding to the peak in experimental VA, and cz_4 is the Zernike coefficient corresponding to defocus, with the normalization given by the ANSI standards (American National Standards Institute (ANSI), 2004). After these calculations, it was found that for most subjects, the model predicted a peak in VA for a non-zero defocus, D_{0_model} in diopters, in agreement with the findings of Yoon and Williams. Therefore, assuming that the defocus state that maximizes the measured VA is the same that maximizes the predicted VA, we selected D_{0_model} to be the actual defocus at the peak of both experimental and predicted VAs. We shifted the experimental curve to have its peak located at D_{0_model}, and we performed again the model calculations to mimic the experimental conditions (pupil size variations and optotypes presented) for each refractive state tested experimentally with a new assigned defocus Zernike term

$$cz_4 = \frac{r^2}{4\sqrt{3}}(D_{lens} - D_0 + D_{0\_model}). \quad (6)$$

The new formulation was such that at the experimental VA peak (D_{lens} = D_0), the Zernike defocus term in the model calculations was equal to $r^2 D_{0\_model}/4\sqrt{3}$ and hence yielded the predicted peak. The Zernike defocus terms for the other refractive states were derived from this position. This methodology resulted in having two VA curves, experimental and predicted, with matching peaks located at the defocus term that balances the other natural aberrations and maximizes the predicted VA for the stimulus spectrum.

Results

Ocular aberrations

Figure 3 shows for each eye tested the median pupil diameter and the ocular aberrations (excluding defocus) in terms of wavefront error RMS. The RMS was calculated with the Zernike coefficients, which were scaled from the pupil diameter of the wavefront measurements to the median pupil diameter measured during the VA measurements (Schwiegerling, 2002). The median pupil was chosen for these calculations as a more robust estimator

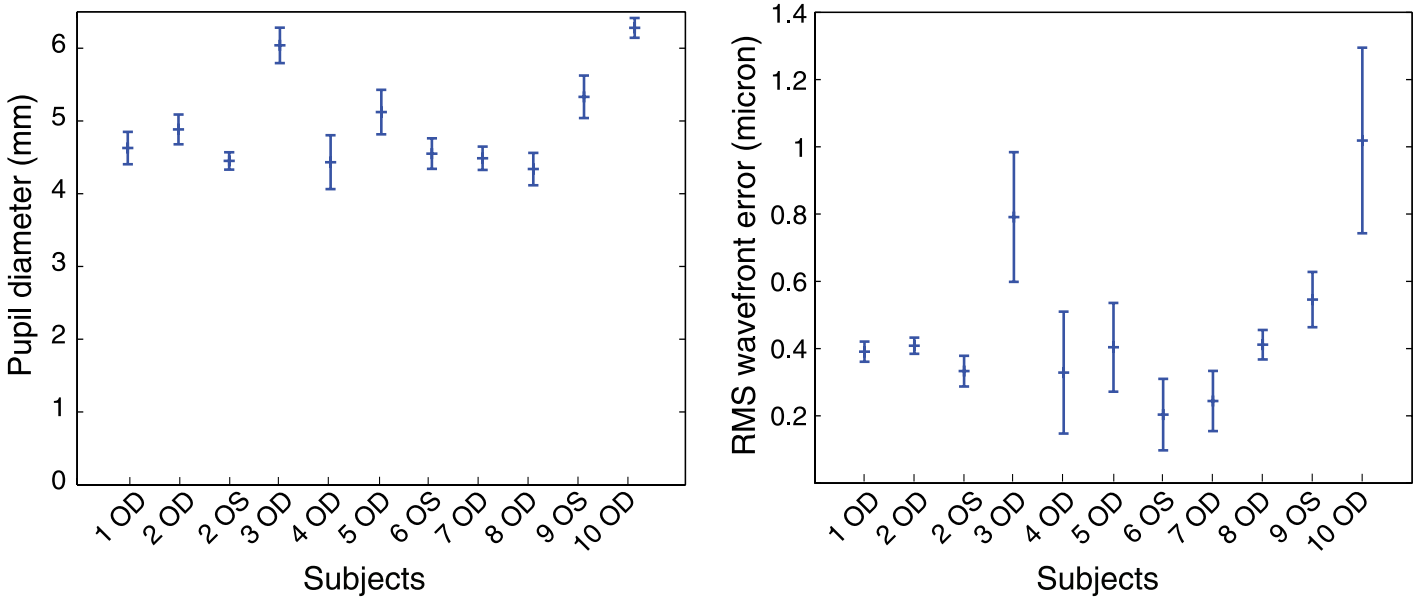

Figure 3. (a) Median pupil diameter and (b) ocular aberrations of the subjects (excluding defocus) over the median pupil. The error bars represent ±1 standard deviation.

than the average. It should be clarified here that the method of Zernike coefficient scaling was not used in the model calculations; instead the wavefront reconstructed over the measurement pupil was cropped to the pupil measured during the visual test, as explained earlier. The graphs also show the standard deviation of the pupil diameter during the through-focus visual acuity test and the standard deviation of the RMS for each subject; each of those was calculated with the median pupil diameter for each refractive state. The aberrations shown include astigmatism and higher order aberrations (from the third Zernike radial order). The latter represents between 0.1 and 0.21 μm wavefront error RMS, except for Subject 3 OD (0.4 μm RMS) and Subject 10 OD (0.61 μm RMS). The error bars of the RMS plot show significant variations for some subjects, due to the changes in pupil diameter during the visual test.

Predicted and measured visual acuities

It was mentioned in the Methods section that without knowledge of the absolute defocus term to be included in the model calculations, the approach was taken to match the predicted best focus position to the experimental peak in VA. Figure 4 illustrates this procedure for Subject 4. The initial calculations, based on a defocus term equal to 0 at the experimental VA peak, yielded for that subject a predicted VA peak at a position 0.5 D from the experimental peak position (see red arrows in Figure 4a). Hence, we shifted the experimental curve along the x-axis to have its peak matched with the predicted peak, and the predictions were updated to take into account the experimental parameters associated with each refractive state (see Figure 4b). For example, the model prediction for the visual acuity at the peak of the experimental curve now includes a defocus term equal to 0.5 D. It is also based on the optotypes presented during the visual test that gave this experimental VA value and the aberration pattern reconstructed over the pupil diameter measured during that same test. The implementation of these parameters in the model is part of the approach taken to mimic tightly the experimental conditions. It can be noted that the predicted VA at 0.5 D in Figure 4b is slightly different to that for the same defocus value in Figure 4a because the latter was calculated with the experimental parameters (pupil diameter and optotypes) associated with a different VA visual test. The predicted VA curve now encompasses a different range of defocus values, and its shape is slightly altered.

The comparison of experimental and predicted visual acuities for all subjects, after the curve shifting as detailed above, is shown in Figure 5. The values represent the mean over four measurements or simulations. The visual acuity is plotted as a function of the defocus term of the ocular aberrations, calculated according to Equation 6 and expressed here in diopters: $D_{graph} = D_{lens} - D_0 + D_{0\_model}$.

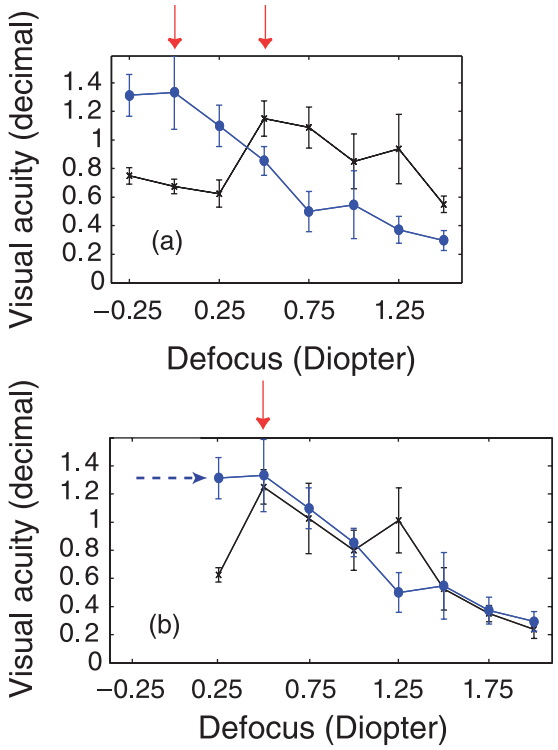

Figure 4. VA peak matching. (a) Experimental (blue, °) and predicted (black, ×) visual acuities with defocus referenced from the experimental VA peak (see Equation 5). (b) Experimental curve shifted to match the model peak and predictions recalculated to fit the experimental parameters (see text). The error bars represent ±1 standard deviation of the four VA measurements or predictions.

It can be seen on the graphs that the experimental and predicted maximum of visual acuity is often at a defocus value different to zero. This is due to the fact that some amount of defocus can compensate for the other aberrations, as mentioned earlier. The points to the left of the experimental peak in visual acuity, in the hyperopic range, must be considered with caution because the subject could accommodate to compensate the effect of the ophthalmic lens, and that was not taken into account in the model. These points were removed for the subsequent analysis of the results.

The RMS error between the decimal experimental data and the predictions over all the subjects is 0.23, and the correlation coefficient R is 0.79. The goodness of the model fit is subject-dependant. For some subjects (e.g., Subject 5), the model predictions follow closely the measured VA, while for some others (e.g., Subjects 1 OD and 2 OS), the discrepancy is higher between the two curves. When selecting the peak VA values for each subject, the correlation between predictions and experimental data is decreased to 0.5. This finding is in agreement with a study highlighting a lack of correlation between visual acuity at the best subjective refraction and the amount of higher order aberrations (Villegas, Alcón, &

Artal, 2008). In the Methods section, we detailed the procedure employed to match the peak of both experimental and model curves. It might be hypothesized that this method is not the most appropriate for some of the subjects, for whom the model curve exhibits several maxima of close values (e.g., Subjects 1 OD and 2 OS). An alternative approach, which consists in shifting the two curves to minimize the RMS error between the model and the experimental data for each subject, lowers the overall RMS error to 0.19. The last plot in Figure 5 shows the experimental and model VA group average, taken from the best focus position of each subject. The close agreement between the two curves illustrates the efficiency of the model. One might notice that the average predicted VA values are slightly lower than the measured ones. It was found that scaling the predictions by a factor of 1.03 for a least-square fit of the whole data set could only lower the overall RMS error by less than 1%. Discrepancies between the model and the experimental curves might be explained by inappropriate generic

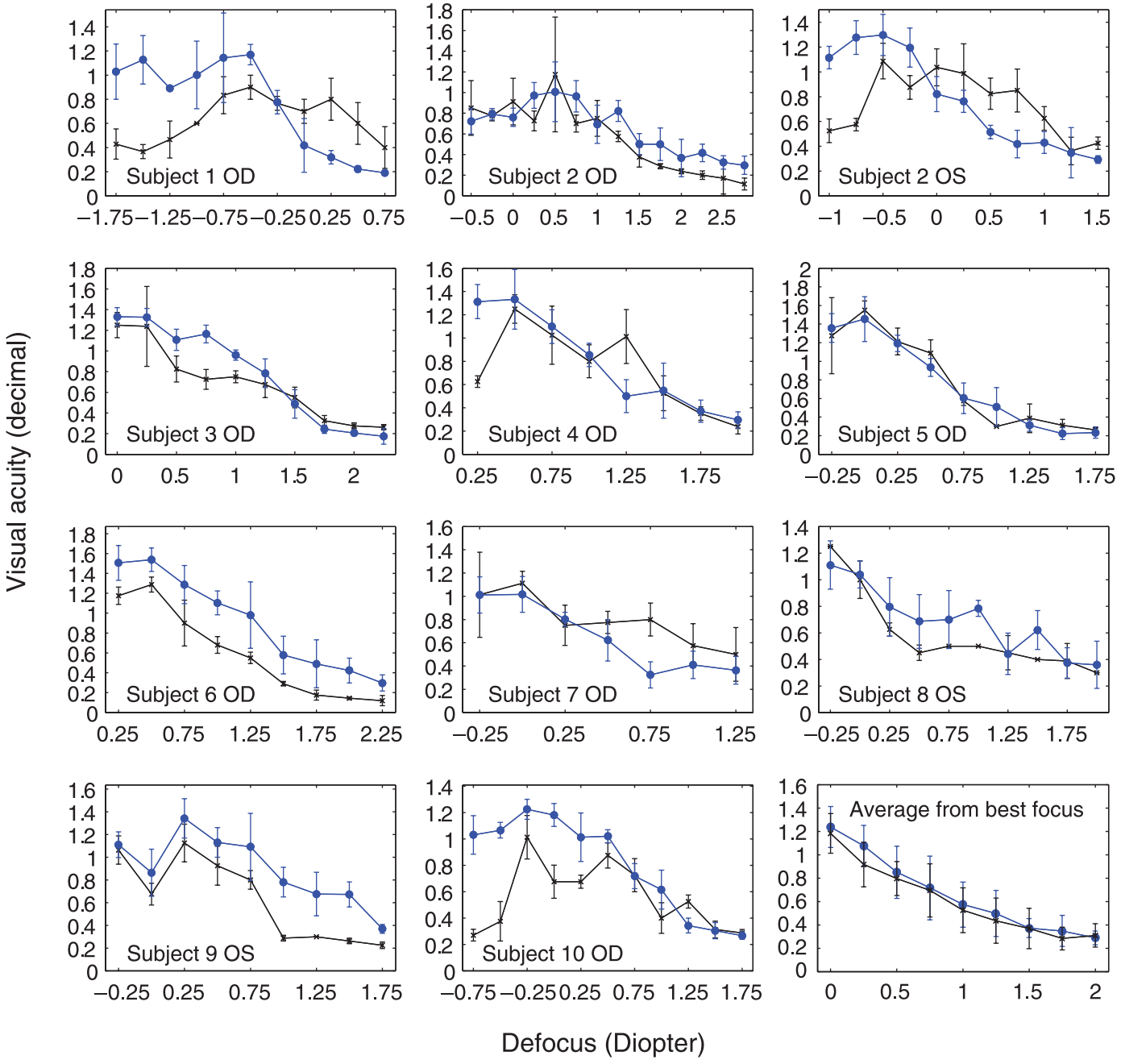

Figure 5. Comparison of the experimental (blue, °) and model (black, ×) visual acuities for all subjects; the error bars represent ±1 standard deviation of the four VA measurements. Bottom right subplot: Group average VA for each defocus position from the best focus; the error bars represent ±1 standard deviation of the group VA measurements.

parameters, or the omission of specific features in the model. The effect and the tolerances of each particular stage of the model on the model predictions will be analyzed in the Discussion section.

An important feature of this work is that a large range of aberration levels was examined. Hence, it provides insight into the robustness of the model with the level of aberration, in this case mainly defocus. In order to quantify the depth of focus of the curves, the standard deviation was calculated as

$$STD_{Focus} = \left[\frac{\sum_D VA(D) \times \left(D - D_{peak}\right)^2}{\sum_D VA(D)}\right]^{0.5}, \quad (7)$$

where D is the defocus value in diopters, D_{peak} is the value of defocus where the peak in VA was obtained, and $VA(D)$ is the VA at defocus D. For both experimental and model curves, the calculation was performed for each subject and then averaged. With this method, the mean depth of focus was estimated to be 0.82 D for the experimental VA and 0.83 D for the model VA. Hence, the model predicts a depth of focus very close to the experimental one.

Discussion

The results show that our customized Bayesian model of visual acuity predicts values very close to the experimental data. In the following, we will compare the efficiency of the model to image quality metrics and other visual process models. We will also discuss the importance and the possible improvements for each stage of the model.

Comparison with image quality metrics

In order to appreciate the performance of the model to predict visual acuity, we compared it with metrics of optical quality derived from the ocular wavefront measurements. Several metrics have previously been assessed and have shown good correlation with subjective judgment of best refraction (Cheng, Bradley, & Thibos, 2004; Guirao & Williams, 2003; Thibos et al., 2004) or visual acuity (Marsack, Thibos, & Applegate, 2004). Among the metrics showing high correlation coefficients with the data, we chose STD and SM to represent the intensity and spatial spread of the point spread function (PSF), and NS and VSMTF to represent the visual Strehl ratio in the image and Fourier domain. In addition, we computed the following metrics: $RMS_W{}^{-1}$, the inverse of the wavefront error RMS, SFcMTF, to express the highest spatial frequency passed by the visual system, and VASmith, based on the simple relation between visual acuity and defocus, with the pupil diameter as an additional variable (Smith, 1991). The latter metric was calculated on the basis that Smith's simple relation has been used to describe through-focus visual acuity. The metrics' definitions and formulas are given in Appendix A. The metrics were calculated with the polychromatic OTF based on the wavefront aberrations reconstructed over the median of the pupil diameter measured for each defocus value. When appropriate, the same generic neural transfer function was used as in the model calculations. The metrics were calculated for a range of defocus values in steps of 0.25 D. In the case of VASmith, it was calculated from the overall median pupil diameter and the defocus amount in diopters added from the refractive state giving maximum acuity. All the metric values were directly compared to the experimental visual acuity values. In accordance with the model readjustments, the metric predictions were shifted along the defocus axis to match their peak with the experimental VA peak.

Figure 6 shows the correlation between the metrics/model predictions and the experimental data. As evidenced by the correlation coefficients, the model and several metrics calculated here demonstrate relatively good correlation with the data. The overall best correlation is obtained with the model, while SM and SFcMTF give the best correlation among metrics. The other metrics all have a correlation coefficient above 0.5, with the lowest given by STD. For several metrics, the spread of the points is not constant with visual acuity. In particular, STD, NS, VSMTF, and VASmith show a bigger spread of points at high visual acuity than at low visual acuity. The correlation coefficient drops down when looking at the peak VA values only. It is 0.34 (R^2 = 0.12) for $RMS_W{}^{-1}$, a value close to that found by Villegas et al. (2008) between best-corrected high contrast VA and wavefront error RMS (R^2 = 0.13). For the other metrics, we found even lower or not statistically significant correlation, again in agreement with Villegas et al. It should be noted that for this restricted set of experimental data, the model still performed better than the metrics (R^2 = 0.25), showing the advantage of modeling the whole visual task for these particular conditions.

A key feature of our customized Bayesian model is that it outputs an absolute prediction of visual acuity. The calculation is based on a model of early visual processes and a computer simulation of the experiment. The metrics, on the other hand, provide a simple number that can be related to the experimental visual acuity. For further comparison of the model with the metrics, we scaled each metric to minimize the RMS error with the experimental data. The resulting minimized RMS errors are shown with the RMS error calculated for the model in Figure 7. Once again, the model performs slightly better than the metrics SM and SFcMTF, and the worse metrics are here NS and VSMTF.

We also calculated the mean depth of focus for each metric using Equation 7. The results are given in Figure 8.

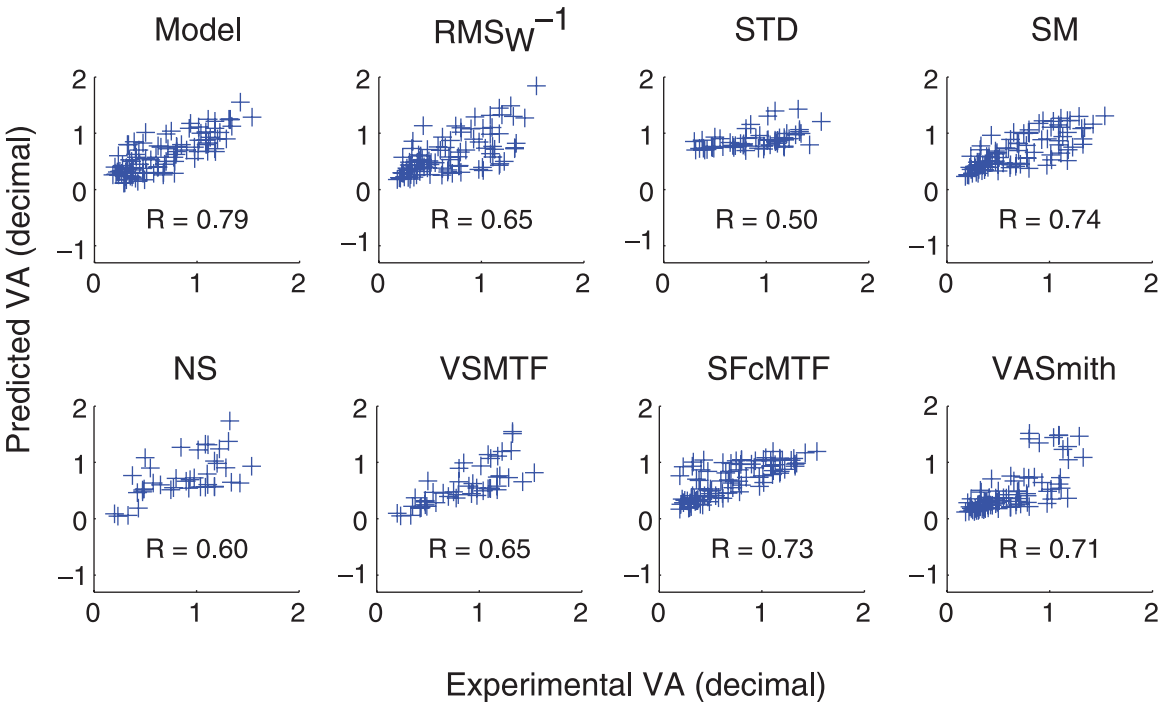

Figure 6. Correlation between the model or the metrics and the experimental data. Each subplot shows the correlation for one metric/model, and the correlation coefficient is given.

The curves for the model and the metrics $RMS_W{}^{-1}$, SM, and SFcMTF have a mean STD_{Focus} very close to the mean of the STD_{Focus} of the experimental curves. The metrics STD, NS, VSMTF, and VASmith tend to underestimate the depth of focus. The relatively good performance of $RMS_W{}^{-1}$ here may be explained by the fact that the aberrations are dominated by defocus for the major part of the VA curve. VASmith, on the other hand, gives poor estimation of the depth of focus as compared to other metrics. This may appear surprising since the metric is based on a relation between spherical refractive error and visual acuity (Smith, 1991). In his paper, Smith mentions that the linear relation between acuity and refractive error is not valid at low levels of refractive error; this may explain the discrepancy observed.

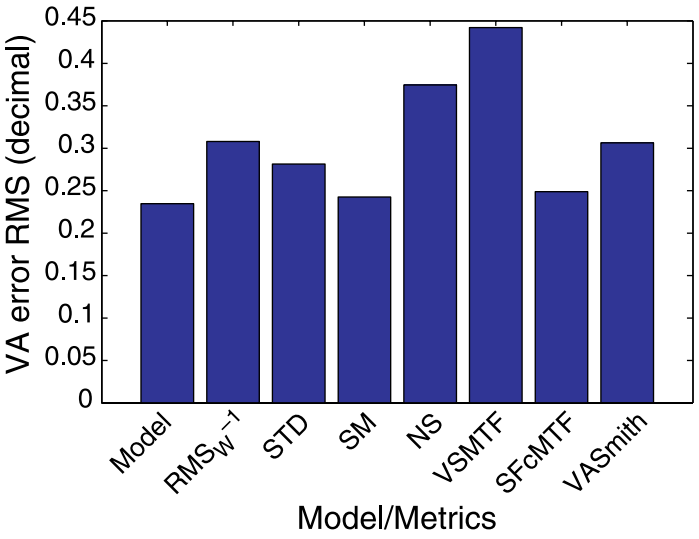

Figure 7. RMS error between the model or scaled metrics and the data.

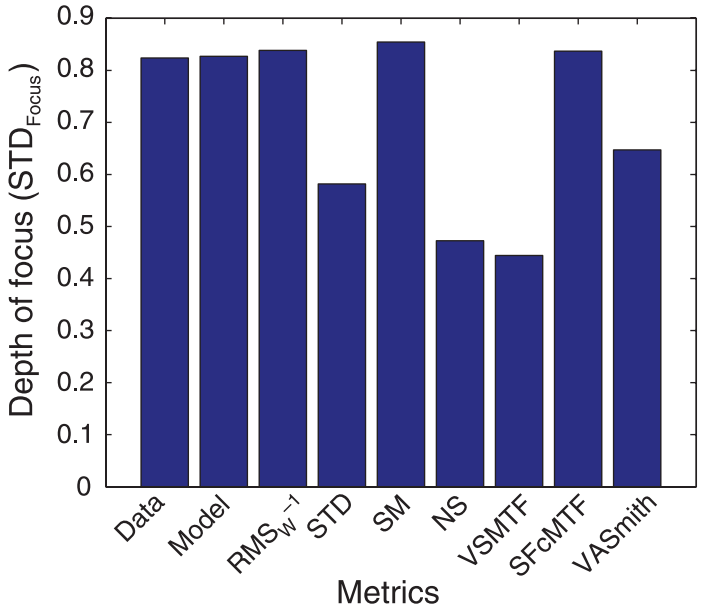

Figure 8. Mean standard deviation of the visual acuity curves as a function of defocus.

Comparison with other early visual process models

As mentioned above, an important point of the model is that it does not require any fit, as it gives an absolute prediction of visual acuity. This is an invaluable advantage over the metrics that provide just relative figures of merit for visual performance. It also describes all the early visual processes leading to the subject's response to a physical stimulus.

Recently, Watson and Ahumada (2008) showed that with knowledge of ocular aberration data, visual process models could give a very good fit of visual acuity measurements. They predicted visual acuity with different model strategies for a set of ocular aberrations and compared the results with measured visual acuity when the aberrations were simulated (Cheng et al., 2004). After optimization of the internal noise level and of the spatial frequency parameters of the NTF for each observer separately, they found correlation coefficients between experimental data and predictions of over 0.86 for all model strategies tested. The minimum RMS error obtained for the best model variation was 0.06 LogMAR (correlation coefficient of 0.91). The acuity metric derived in the paper yielded, again after fitting of the noise level and the frequency scale, an RMS error of 0.07 and a correlation coefficient of 0.86. In comparison, the RMS error between our predictions and our measurements amounts to 0.15 LogMAR. Our model differs to the classical models used by Watson and Ahumada in several ways. Firstly, in a classical ideal observer model, the model observer compares the cortical image to the possible templates (either filtered or ideal) and chooses one of them according to a matching rule. In the present model, the observer is unaware of the optical degradation, which is implicitly estimated by the Bayesian pattern recognition method. It could be noted that this approach is somehow in between the matched (aberrated template) and unmatched (ideal or diffraction-limited template) strategies as presented by Watson and Ahumada. This affects the observer's efficiency in performing the visual task, but we believe our approach is more representative of normal vision. Another major difference is that the neural noise in our model is implemented by the neural contrast threshold that is applied to the channel response. Thus, the model provides an absolute estimate of visual acuity, without the need for noise adjustment, as is done in Watson and Ahumada's study. Finally, it can be noted that the set of aberrations used in their study only included pairs of Zernike coefficients (defocus/spherical aberration and primary astigmatism/secondary astigmatism), while our data set comprised a variety of natural ocular aberrations. We also investigated a larger number of subjects as well as a larger range of aberration amounts. These features might explain why the RMS error found in our study is higher than that found by Watson and Ahumada with the different versions of their model and acuity metric. However, we wish to emphasize again that our model calculations were performed without any noise or neural spatial frequency adjustment. In a similar approach to that followed by Watson and Ahumada, we could have adjusted the other parameters of the model to obtain a better fit with the experimental data. Such a post-processing of the results was not felt necessary as the results obtained were reasonably good. The efficiency of our partially customized model might not be optimal for each observer but is still very good over a large number of subjects and aberration conditions. This is crucial as regards to the usefulness of an absolute visual acuity prediction.

Looking again at the last panel in Figure 5, one can see a close match between averages of measurements and predictions. For some subjects, we can also observe such close agreement. In other words, our absolute predictions (without any model parameter fit) show a high fidelity for averages and for some subjects but can show significant discrepancies in some cases. This suggests that intersubject variability occurs not only in wave aberration (the customized part of the model) but probably occurs as well in other visual stages not customized so far. The model itself does not preclude further customization. One could use additional subject data (cone sampling, NTF, etc.) when available, or even use some parameters to fit the data. In the following, we will discuss the effect of each model feature and potential predictive improvements with further customization.

Effect of the model features on the predictions

The model of visual acuity, as presented in this paper, is partially customized. The monochromatic OTF is based on aberrometric measurements, but the polychromatic OTF is based on a generic model (Thibos et al., 1992) and so is the retinal sampling simulation, as well as the neural transfer function (Losada et al., 1993). We will now examine each stage of the model in order to appreciate its effect on the model predictions and propose some possibilities of further customization.

Retinal image formation

The first stage of the model is retinal image formation, calculated from aberrometric data and a longitudinal chromatic aberration model. One might question the importance of ocular aberrations other than defocus in experimental conditions dominated by the latter. Therefore, we performed the calculations with defocus only included in the model. Again, we shifted the predicted curve to match its peak with the experimental peak. It was found that the fit to the experimental data was much worse in these conditions, as easily evidenced by Figure 9.

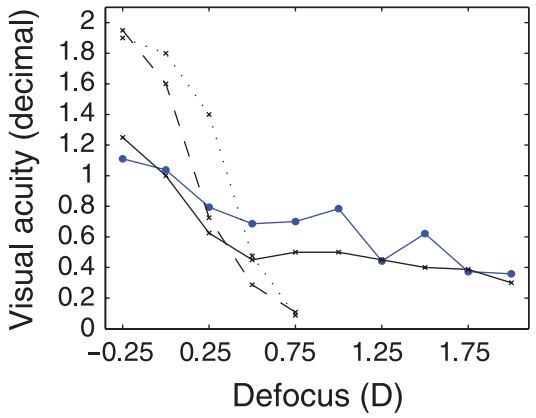

Figure 9. Effect of defocus on model predictions: Measured VA (blue, °, solid line), predicted VA with all aberrations (black, ×, solid line), predicted VA with defocus only (black, ×, dashed line), and predicted VA with defocus and population average spherical aberration (black, ×, dotted line), for Subject 8 OS. The model limitations did not enable to calculate VA with defocus only nor with defocus and spherical aberration, after 0.75 D from the best focus position.

Subject 8 taken for this example had an initial wavefront error RMS corresponding to the median of the wavefront error RMS of all subjects. With defocus only included in the model, the predicted VA is much higher when in-focus and decreases much more rapidly away from it than when all aberrations are taken into account. In fact, the predicted VA decreased so rapidly that a limit was quickly reached as the model could not cope with such low retinal image quality. The trend is in agreement with recent studies showing an increase of in-focus visual performance and a decrease in depth-of-focus with adaptive optics correction of ocular aberrations (Guo, Atchison, & Birt, 2008; Piers, Manzanera, Prieto, Gorceix, & Artal, 2007). We also performed the calculations with a population average of spherical aberration, the only Zernike coefficient with a non-zero population average (Thibos, Hong, Bradley, & Cheng, 2002). From the literature (Applegate, Donnelly III, Marsack, Koenig, & Pesudovs, 2007), we selected the mean spherical aberration RMS measured for a population matching our age and pupil size group; this was found to be 0.065 μm. The predicted VA in these conditions shows a slightly wider depth-of-focus, although it still decreases much more rapidly than the experimental VA and than that predicted with the natural aberrations of the subject. In the context of our model predictions, it demonstrates the importance to take into account ocular aberrations, even if large amounts of defocus were added in the experiments.

Having stated the importance of the modeling of monochromatic aberrations, it is worth analyzing the limitation and possible customization of this stage. Care was taken to take into account the variations due to the pupil time-dependent dilation, as the wavefront was truncated to the pupil size for each letter size tested. It was noted from Figure 3 that the pupil size variations had significant impact on the wavefront error RMS for some subjects. One might argue that the reconstruction is based on the assumption of a concentric dilation of the pupil, which may not hold true for all subjects (Wilson, Campbell, & Simonet, 1992). The model could thus be improved with a measurement of the pupil center shift with dilation. Although we did not consider possible changes of the aberrations during the VA test (except those due to pupil variations), we believe that the main error on monochromatic aberrations probably arises from the uncertainty on the defocus term, as detailed in the Methods section. It can also be noted that the shifting fit remains limited to the fact that both model and experimental curves have a 0.25-D sampling.

A further step in the customization of the model is to take into account the Stiles–Crawford (SC) effect. We performed the model calculations with an apodization function on the pupil plane (Applegate & Lakshminarayanan, 1993) to implement that effect. Figure 10 shows that for a small natural pupil (4.3-mm diameter for Subject 8) the inclusion of the SC effect in the model yields small differences. Bigger discrepancies might have been expected for a bigger natural pupil (6.3-mm diameter for Subject 10); however, it can be seen from Figure 10 that the impact of the SC effect on the model predictions remains limited even for the biggest pupil in our experiment. Perhaps the latter pupil size is at the limit for the SC effect to have significant influence on the model predictions. It can also be hypothesized that the SC effect may have impact on contrast rather than on acuity, on which the visual test was based. It was found that over all subjects, the RMS error between the model predictions of VA and the experimental values was very similar whether the SC effect was taken into account or not. The impact of the SC effect on the retinal image quality is dependent on the location of the SC peak, and this would in turn certainly affect the model predictions. Hence, without knowledge of the SC effect parameters for each subject, we chose to keep the predictions without the modeling of the SC effect.

As for chromatic aberrations, their importance was already pointed out in the first paper on the model (Nestares et al., 2003): The superiority of polychromatic predictions over monochromatic predictions was demonstrated. In the current version of the model, a finer sampling of the polychromatic OTF was used. It was found that the finer sampling (every 10 nm, corresponding to 30 wavelengths) yielded minimal changes in the model predictions as compared to the coarse sampling (only 3 wavelengths used). This could have been inferred from the results shown by Ravikumar, Thibos, and Bradley (2008): They highlight that while a 10-nm sampling is required to avoid calculation artifacts in conditions close to the diffraction limit, low sampling is adequate for aberrated eyes.

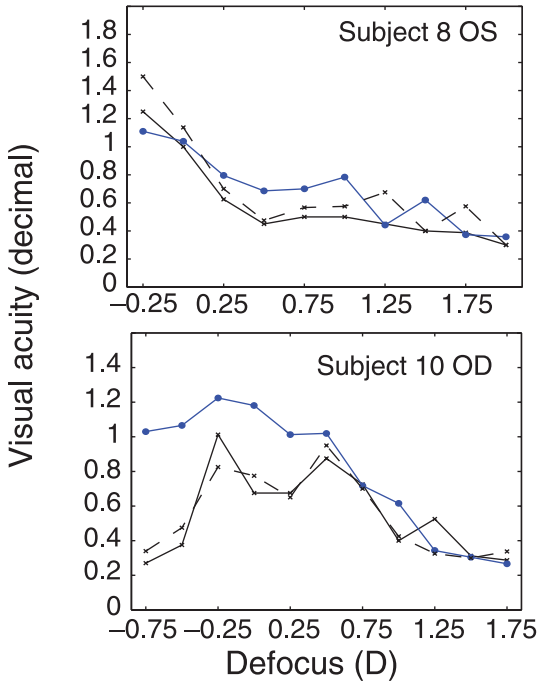

Figure 10. Stiles–Crawford effect and model predictions: Measured VA (blue, °, solid line), predicted VA without SC effect (black, ×, solid line), and predicted VA with SC effect (black, ×, dashed line), for Subject 8 OS (4.3-mm diameter pupil) and Subject 10 OD (6.3-mm diameter pupil).

Finally, while we considered longitudinal chromatic aberrations (LCAs), transverse chromatic aberrations (TCAs) were ignored. The reasons were that the literature shows a large intersubject variability in the TCA amount (Rynders et al., 1995) and that a proper characterization of TCA for our subjects would have implied long and tedious psychophysical experiments. This customization, out of the scope of the present paper, could potentially improve the efficiency of the model. It is expected, however, that the change in the model predictions would be minimal as it appears from the literature that TCA has very little effect on image quality when added to LCA for normal aberrated eyes (Marcos, Burns, Moreno-Barriusop, & Navarro, 1999; Ravikumar et al., 2008).

Retinal sampling

The next step in the model is the sampling of the retinal image by the photoreceptor mosaic. As mentioned earlier, we used in the model the mean cone density measured anatomically at the fovea (Curcio et al., 1990). We investigated the effect of this stage on the model predictions, by removing it in the model calculations, and alternatively by reducing the cone sampling by 33% to reflect the large intersubject variations that have been measured (Curcio et al., 1990; Marcos, Navarro, & Artal, 1996). Figure 11 shows an example of these calculations for Subject 8. The omission of the sampling stage in the model does not yield noticeable changes in the results: The predicted VA curve is merged to the initial one. In fact, after similar calculations for all subjects, we found an RMS error to the experimental data equal to that originally obtained. Figure 11 also shows that reducing the cone sampling frequency by 33% results in small and non-monotonic differences in the model predictions. The potential detrimental effect of under-sampling by the cone mosaic (when the retinal image spectrum extends beyond the Nyquist limit defined by the cone mosaic) is aliasing. Our results indicate that the normal range of human cone sampling frequencies does not produce aliasing of images in the experimental conditions studied. This confirms the statement that the optics of the eye and the cone mosaic are well matched to prevent aliasing in normal viewing conditions (Williams, 1984). Additional tests in the absence of ocular aberrations, or with a smaller modeled cone density, showed a decrease of predicted visual acuity, as expected. It can be concluded that the cone sampling has no significant effect on the model predictions for our experimental conditions. However, in view of using the model in other conditions of ocular aberrations (for example, with very low amounts of aberrations), it is preferable to maintain this stage in the model.

Cortical image representation

In the model, the sampled retinal image is filtered by a set of Gabor channels, and a contrast threshold, derived as the inverse of the neural transfer function (NTF), is applied to the channel responses. The channels are fundamental to the model as they ensure the simplicity and stability of the pattern recognition algorithm. Therefore, they cannot be removed easily for testing purposes. The variety of parameters defining the filter bank

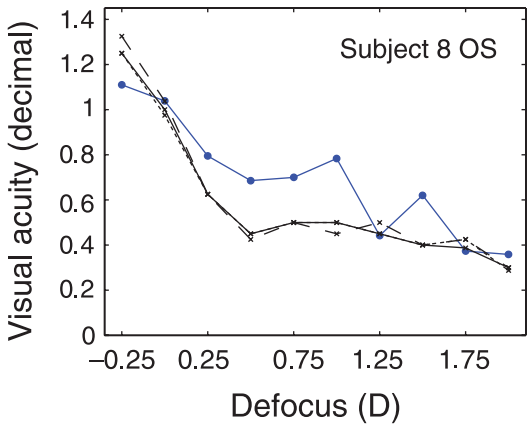

Figure 11. Effect of cone sampling on model predictions: Measured VA (blue, °, solid line), predicted VA with 120-cpd cone sampling frequency (black, ×, solid line), predicted VA with 80-cpd cone sampling frequency (black, ×, dashed line), and predicted VA without cone sampling (black, ×, dotted line) for Subject 8.

(functions, bandwidth, number, distribution) makes it impractical to study their effects on the model predictions. It should be noted, however, that they were chosen to be biological plausible and they are suitable to our spatial domain implementation (Nestares et al., 1998).

The NTF can be more easily manipulated. Similarly to the cone density, it is known to vary from subject to subject (Losada et al., 1993; Williams, 1985). In this context, we ran some tests to appreciate the effect of the NTF on the model predictions: in particular, when it is ignored in the model (i.e., equal to unity for all spatial frequencies), and when the original function taken from Losada et al. (1993) is divided by 2. The results for Subject 8 (see Figure 12) show that the omission of the NTF mainly has an impact on the model predictions near the in-focus position. The RMS error between the predictions with unit NTF and the experimental data for all subjects is about twice that obtained with the initial NTF. When the NTF is divided by 2, the predicted VA is slightly decreased. In other simulations, much bigger changes were noticed when the NTF was attenuated by 90%. Further tests would imply varying the shape of the NTF, but again, this is not practical in the context of our model calculations. It is expected, from these preliminary simulations, that customizing the NTF for each subject (with psychophysical measurements) could improve the fit to the experimental data.

Bayesian pattern recognition

Finally, we did not investigate variations in the Bayesian pattern recognition scheme, which is also dependant on the channel filtering, as this would imply major changes in the model. It was beyond the scope of the present paper but could be investigated in a future study. It could be noted, for example, that one aspect that could explain the discrepancies between data and model results is the possibility that some subjects might have developed some level of adaptation or learning of their usual degraded retinal images, as could be suggested by some reported evidence (Artal et al., 2004; Chen, Artal, Gutierrez, & Williams, 2007). Furthermore, three of the subjects (Subjects 3, 9 and 10), for whom the predicted VA is generally lower than the measured VA, are co-authors of the present paper and may have benefited from better training/knowledge of the visual test.

To conclude on this analysis of the model stages, it appears that for our particular data set, the fine modeling of ocular aberrations is crucial for the effectiveness of the predictions. In particular, it is worth noting that all monochromatic aberrations (including astigmatism and higher order aberrations) needed to be taken into account, even if the experiment was a through-focus paradigm with relatively large amounts of defocus. The photoreceptor sampling did not seem to have an impact on the model results but that could be explained by important reduction in the high spatial frequency range due to optical aberrations. The NTF mostly affects the predictions close to the in-focus position (when the aberrations are small), but a customization of this function for each subject could well improve the model efficiency. Our results suggested a lower correlation between predictions and measured VA when in-focus, supporting a recent study demonstrating the lack of strong correlation between ocular optical quality and best-refracted visual acuity (Villegas et al., 2008). Although the model outperforms the metrics in these conditions, it would certainly be of interest to investigate further the neural stages to improve its predictive power.

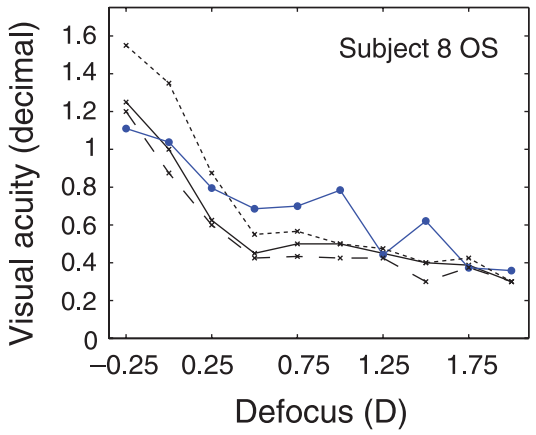

Figure 12. Effect of NTF on the model predictions: Measured VA (blue, °, solid line), predicted VA with NTF from Losada et al. (1993; black, ×, solid line), predicted VA with NTF divided by 2 (black, ×, dashed line), and predicted VA with a unit NTF (black, ×, dotted line) for Subject 8.

Conclusion

We presented an experimental validation of a partially customized Bayesian model of visual acuity with a large range of natural aberrations and induced defocus and eleven tested eyes. The model predicted values of visual acuity are in close agreement with the experimental data and outperformed optical quality metrics. It presents the invaluable advantage of yielding an absolute prediction of visual acuity, without the need for any adjustment (noise level, etc.). It also provides a physically explicit schematic of the mechanisms involved in vision. In that context, we investigated the effect of individual stages on the overall model output. This analysis highlighted the importance of a fine modeling of ocular aberrations and the potential improvement of the model predictive power with a customization of the neural transfer function. Our model of visual acuity can have important clinical applications as an efficient predictor of visual acuity in various

conditions, while also strengthening our understanding of visual processes.

Appendix A

For the interest of readers, we transcribe here the definitions and derivations of the metrics used for this work, according to the original paper by Thibos et al. (2004). The last metric, VASmith, was reformulated from the original paper by Smith (1991).

RMS_W^{-1}: inverse of the RMS of the wavefront error, which is given as

$$RMS_W^{-1} = \left(\sqrt{\int_{pupil} W(x,y)^2 dxdy} \right)^{-1}. \quad \text{(A1)}$$

STD: standard deviation of the intensity values of the point spread function (PSF), which is given as

$$STD = \frac{\left[\int_{image} \left(PSF(x,y) - \overline{PSF} \right)^2 dxdy \right]^{0.5}}{\left[\int_{image} \left(PSF_{DL}(x,y) - \overline{PSF}_{DL} \right)^2 dxdy \right]^{0.5}}. \quad \text{(A2)}$$

SM: standard deviation of the PSF spatial distribution, which is given as

$$SM = \left[\frac{\int_{image} (x^2 + y^2) \times PSF(x,y) dxdy}{\int_{image} PSF(x,y) dxdy} \right]^{0.5}. \quad \text{(A3)}$$

NS: neural sharpness, Strehl ratio of the PSF weighted by a spatial sensitivity function $g(x, y)$, which is given as

$$NS = \frac{\int_{image} PSF(x,y) g(x,y) dxdy}{\int_{image} PSF_{DL}(x,y) g(x,y) dxdy}. \quad \text{(A4)}$$

VSMTF: visual Strehl ratio computed in the spatial domain with the MTF, which is given as

$$VSMTF = \frac{\int_{fourierimage} NTF(f_x,f_y) \cdot MTF(f_x,f_y) df_x df_y}{\int_{fourierimage} NTF(f_x,f_y) \cdot MTF_{DL}(f_x,f_y) df_x df_y}. \quad \text{(A5)}$$

SFcMTF: spatial frequency cutoff of radially averaged modulation-transfer function (rMTF), i.e., intersection of rMTF with the neural contrast threshold (NCT), which is given as

$$rMTF(SFcMTF) - NCT(SFcMTF) = 0. \quad \text{(A6)}$$

VASmith: visual acuity calculated according to the formula by Smith, which states the proportionality between the minimum angle of resolution and the product of the pupil diameter Φ with the refractive error E (Smith, 1991). Using the proportionality constant given in the cited paper, it gives for decimal VA

$$VASmith = \frac{1}{0.83 \times \Phi \times E}. \quad \text{(A7)}$$

Acknowledgments

This work was supported by the Comisión Interministerial de Ciencia y Tecnología, Spain, under Grants FIS2005-05020-C03-01 and FIS2008-00697. The authors further acknowledge the support of the Science Foundation Ireland under Grant SFI/07/IN.1/1906 (E. Dalimier), the Spanish Ministerio de Educacion y Cultura under FPU Scholarship No. AP2004-0122 (E. Pailos), and Programme Alban, the European Union Programme of High Level Scholarships for Latin America under Scholarship No. E07D402088CL (R. Rivera). The authors would like to thank J. Arines for his help with the commercial (Tracey) aberrometer. They are also grateful to C. Dainty and the anonymous reviewers for their comments on the manuscript.

Commercial relationships: none.
Corresponding author: Eugénie Dalimier.
Email: eugenie.dalimier@nuigalway.ie.
Address: Applied Optics Group, School of Physics, NUIG, Galway, Ireland.

References

American National Standards Institute (ANSI) (2004). *American national standard for ophthalmics—Methods for reporting optical aberrations of eyes* (vol. ANSI Z80.28). Washington, DC: ANSI.

Applegate, R. A., Donnelly, W. J., III., Marsack, J. D., Koenig, D. E., & Pesudovs, K. (2007). Three-dimensional relationship between high-order root-mean-square wavefront error, pupil diameter, and aging. *Journal of the Optical Society of America A, Optics and Image Science, 24,* 578–587. [PubMed] [Article]

Applegate, R. A., & Lakshminarayanan, V. (1993). Parametric representation of Stiles–Crawford functions:

Normal variation of peak location and directionality. *Journal of the Optical Society of America A, Optics and Image Science, 10,* 1611–1623. [PubMed]

Artal, P., Chen, L., Fernández, E. J., Singer, B., Manzanera, S., & Williams, D. R. (2004). Neural compensation for the eye's optical aberrations. *Journal of Vision, 4*(4):4, 281–287, http://journalofvision.org/4/4/4/, doi:10.1167/4.4.4. [PubMed] [Article]

Chen, L., Artal, P., Gutierrez, D., & Williams, D. R. (2007). Neural compensation for the best aberration correction. *Journal of Vision, 7*(10):9, 1–9, http://journalofvision.org/7/10/9/, doi:10.1167/7.10.9. [PubMed] [Article]

Cheng, X., Bradley, A., & Thibos, L. N. (2004). Predicting subjective judgment of best focus with objective image quality metrics. *Journal of Vision, 4*(4):7, 310–321, http://journalofvision.org/4/4/7/, doi:10.1167/4.4.7. [PubMed] [Article]

Curcio, C. A., Sloan, K. R., Kalina, R. E., & Hendrickson, A. E. (1990). Human photoreceptor topography. *The Journal of Comparative Neurology, 292,* 497–523. [PubMed]

Dalimier, E., & Dainty, C. (2008). Use of a customized vision model to analyze the effects of higher-order ocular aberrations and neural filtering on contrast threshold performance. *Journal of the Optical Society of America A, Optics and Image Science, 25,* 2078–2087. [PubMed]

Guirao, A., Porter, J., Williams, D. R., & Cox, I. G. (2002). Calculated impact of higher-order monochromatic aberrations on retinal image quality in a population of human eyes. *Journal of the Optical Society of America A, Optics, Image Science, and Vision, 19,* 1–9. [PubMed]

Guirao, A., & Williams, D. R. (2003). A method to predict refractive errors from wave aberration data. *Optometry and Vision Science, 80,* 36–42. [PubMed]

Guo, H., Atchison D. A., & Birt, B. J. (2008). Changes in through-focus spatial visual performance with adaptive optics correction of monochromatic aberrations. *Vision Research, 48,* 1804–1811. [PubMed]

Liang, J., Grimm, B., Goelz, S., & Bille, J. F. (1994). Objective measurement of wave aberrations of the human eye with the use of a Hartmann–Shack wavefront sensor. *Journal of the Optical Society of America A, Optics, Image Science, and Vision, 11,* 1949–1957. [PubMed]

Llorente, L., Diaz-Santana, L., Lara-Saucedo, D., & Marcos, S. (2003). Aberrations of the human eye in visible and near infrared illumination. *Optometry and Vision Science, 80,* 26–35. [PubMed]

Losada, M. A., Navarro, R., & Santamaría, J. (1993). Relative contributions of optical and neural limitations to human contrast sensitivity at different luminance levels. *Vision Research, 33,* 2321–2336. [PubMed]

Marcos, S., Burns, S. A., Moreno-Barriusop, E., & Navarro, R. (1999). A new approach to the study of ocular chromatic aberrations. *Vision Research, 39,* 4309–4323. [PubMed]

Marcos, S., Navarro, R., & Artal, P. (1996). Coherent imaging of the cone mosaic in the living human eye. *Journal of the Optical Society of America A, Optics, Image Science, and Vision, 13,* 897–905. [PubMed]

Marsack, J. D., Thibos, L. N., & Applegate, R. A. (2004). Metrics of optical quality derived from wave aberrations predict visual performance. *Journal of Vision, 4*(4):8, 322–328, http://journalofvision.org/4/4/8/, doi:10.1167/4.4.8. [PubMed] [Article]

Moreno-Barriuso, E., & Navarro, R. (2000). Laser ray tracing versus Hartmann–Shack sensor for measuring optical aberrations in the human eye. *Journal of the Optical Society of America A, Optics, Image Science, and Vision, 17,* 974–985. [PubMed]

Navarro, R. (2009). Objective refraction from aberrometry: Theory. *Journal of Biomedical Optics, 14,* 024021. [PubMed]

Navarro, R., & Losada, M. A. (1997). Aberrations and relative efficiency of light pencils in the living human eye. *Optometry and Vision Science, 74,* 540–547. [PubMed]

Nestares, O., Navarro, R., & Antona, B. (2003). Bayesian model of Snellen visual acuity. *Journal of the Optical Society of America A, Optics, Image Science, and Vision, 20,* 1371–1381. [PubMed]

Nestares, O., Navarro, R., Portilla, J., & Tabernero, A. (1998). Efficient spatial-domain implementation of a multiscale image representation based on Gabor functions. *Journal of Electronic Imaging, 7,* 166–173.

Pelli, D. G., Robson, J. G., & Wilkins, A. J. (1988). The design of a new letter chart for measuring contrast sensitivity. *Clinical Vision Sciences, 2,* 187–199.

Piers, P. A., Manzanera, S., Prieto, P. M., Gorceix, N., & Artal, P. (2007). Use of adaptive optics to determine the optimal ocular spherical aberration. *Journal of Cataract and Refractive Surgery, 33,* 1721–1726. [PubMed]

Ravikumar, S., Thibos, L. N., & Bradley, A. (2008). Calculation of retinal image quality for polychromatic light. *Journal of the Optical Society of America A, Optics, Image Science, and Vision, 25,* 2395–2407. [PubMed]

Rynders, M., Lidkea, B., Chisholm, W., & Thibos, L. N. (1995). Statistical distribution of foveal transverse chromatic aberration, pupil centration, and angle psi in a population of young adult eyes. *Journal of the*

Optical Society of America A, Optics, Image Science, and Vision, 12, 2348–2357. [PubMed]

Schwiegerling, J. (2002). Scaling Zernike expansion coefficients to different pupil sizes. *Journal of the Optical Society of America A, Optics, Image Science, and Vision, 19,* 1937–1945. [PubMed]

Smith, G. (1991). Relation between spherical refractive error and visual acuity. *Optometry and Vision Science, 68,* 591–598. [PubMed]

Thibos, L. N., Hong, X., Bradley, A., & Applegate, R. A. (2004). Accuracy and precision of objective refraction from wavefront aberrations. *Journal of Vision, 4*(4):9, 329–351, http://journalofvision.org/4/4/9/, doi:10.1167/4.4.9. [PubMed] [Article]

Thibos, L. N., Hong, X., Bradley, A., & Cheng, X. (2002). Statistical variation of aberration structure and image quality in a normal population of healthy eyes. *Journal of the Optical Society of America A, Optics, Image Science, and Vision, 19,* 2329–2348. [PubMed]

Thibos, L. N., Ye, M., Zhang, X., & Bradley, A. (1992). The chromatic eye: A new reduced-eye model of chromatic aberrations in humans. *Applied Optics, 31,* 3594–3600.

Vargas, A., Campos, J., & Navarro, R. (2000). Invariant pattern recognition against defocus based on subband decomposition of the filter. *Optics Communications, 185,* 33–40.

Villegas, E. A., Alcón, E., & Artal, P. (2008). Optical quality of the eye in subjects with normal and excellent visual acuity. *Investigative Ophthalmology & Visual Science, 49,* 4688–4696. [PubMed]

Watson, A. B., & Ahumada, A. J., Jr. (2008). Predicting visual acuity from wavefront aberrations. *Journal of Vision, 8*(4):17, 1–19, http://journalofvision.org/8/4/17/, doi:10.1167/8.4.17. [PubMed] [Article]

Williams, D. R. (1984). Aliasing in human foveal vision. *Vision Research, 25,* 195–205. [PubMed]

Williams, D. R. (1985). Visibility of interference fringes near the resolution limit. *Journal of the Optical Society of America A, Optics and Image Science, 2,* 1087–1093. [PubMed]

Wilson, M. A., Campbell, M. C., & Simonet, P. (1992). The Julius F. Neumueller Award in Optics, 1989: Change of pupil centration with change of illumination and pupil size. *Optometry and Vision Science, 69,* 129–136. [PubMed]

Wyszecki, G., & Stiles, W. S. (1982). *Color science: Concepts and methods, quantitative data and formulae* (2nd ed.). New York: John Wiley & Sons.

Yoon, G.-Y., & Williams, D. R. (2002). Visual performance after correcting the monochromatic and chromatic aberrations of the eye. *Journal of the Optical Society of America A, Optics, Image Science, and Vision, 19,* 266–275. [PubMed]